

Spectral analysis of basaltic asteroids observed by the *Gaia* space mission

Dagmara Oszkiewicz¹,^{1*} Hanna Klimczak,¹ Benoit Carry,² Antti Penttilä³,³ Marcel Popescu⁴,⁴ Joachim Krüger¹ and Marcelo Aron Keniger^{5,6}

¹*Astronomical Observatory Institute, Faculty of Physics, Adam Mickiewicz University, Słoneczna 36, P-60-286 Poznań, Poland*

²*Observatoire de la Côte d'Azur, CNRS, Université Côte d'Azur, Laboratoire Lagrange, 06304 Nice, France*

³*Department of Physics, University of Helsinki, P.O. Box 64, FI-00014 Helsinki, Finland*

⁴*Astronomical Institute of the Romanian Academy, 5 Cutilul de Argint, 040557 Bucharest, Romania*

⁵*Nordic Optical Telescope, Rambla José Ana Fernández Pérez 7, E-38711 Breña Baja, Spain*

⁶*Stellar Astrophysics Centre, Department of Physics and Astronomy, Aarhus University, Ny Munkegade 120, DK-8000 Aarhus C, Denmark*

Accepted 2022 November 21. Received 2022 November 21; in original form 2022 August 24

ABSTRACT

There is a great deal of scientific interest in characterizing the basaltic asteroids (spectrally classified as V-types), as they are the key to understanding planetesimal formation and evolution in the early Solar system. These have long been recognized as parts of the crusts of fully differentiated planetesimals. Thus, their multiplicity, distribution, and physical characteristics are crucial for providing context for and constraining the theoretical evolution models of the Solar system. In this work, we perform spectral analysis with an extended data set of spectral measurements from the ESA *Gaia* mission Data Release 3, thus increasing the sample size of the analysed V-types by more than three times as compared to the literature. Using the data provided by *Gaia*, we identified ~ 2000 possible V-type asteroids. About 350 of them successfully pass our data validation criteria. This sample includes 31 new V-type asteroids beyond 2.5 au and 6 in the Phocaea region. We confirm that the V-type asteroids in the middle and outer part of the main belt show distinct spectral properties compared to typical vestoids. In the inner main belt, we found a great diversity of spectral parameters among the V-types in all populations. Number of asteroids show band depths even greater than that of (1459) Magnya. Furthermore, some objects present 0.9 μm band-centres more than one standard deviation away from the typical value for vestoids. However since the DR3 band centres are often overestimated, those findings are to be confirmed. Overall our results indicate that the inner main belt may contain remnants of multiple differentiated planetesimals, not just (4) Vesta.

Key words: Asteroids – Spectroscopy – minor planets – asteroids: general – techniques: spectroscopic.

1 INTRODUCTION

Planetesimals were the first large solid bodies that formed in the Solar system more than 4.5 billion years ago. Current Solar system evolution theories and abundant meteoritic evidence suggest that there once existed 30–150 different differentiated planetesimals (into an iron core, silicate mantle, and crust) (Burbine et al. 2002; Scott et al. 2009, 2015; Greenwood et al. 2015). They were then collisionally disrupted during later stages of the Solar system evolution. Studies of various isotopes in iron meteorites confirm that these extensive collisions exposed iron cores to cool in a time frame of 7.8–11.7 million years after the formation of calcium–aluminium-rich inclusions (Hunt et al. 2022). Numerical studies constrain the formation location of differentiated planetesimals to the present terrestrial planet region (Bottke et al. 2006) or to a wider formation ranges at orbital locations between 1.3 and 7.5 au (Lichtenberg et al. 2021). The disrupted fragments of planetesimals can be found in the current Main Asteroid Belt and in meteorite collections today. In particular, V-type asteroids are identified as parts of the crusts of thermally evolved planetesimals.

V-type asteroids are immediately recognizable from the spectra by two prominent wide olivine/pyroxene absorption bands at wavelengths around 1.0 and 2.0 μm . The first identified V-type object was the asteroid (4) Vesta, which is the largest object of this taxonomic class and is considered a fossil planetesimal. Due to characteristic spectra, Vesta was immediately linked to howardite–eucrite–diagonite meteorites (HEDs) in the early 1970s (McCord, Adams & Johnson 1970). A few decades later, new V-types started to be found in the vicinity of (4) Vesta and in the near-Earth asteroid population (Binzel & Xu 1993; Burbine et al. 2001; Florczak, Lazzaro & Duffard 2002). Soon, the V-types close to Vesta were recognized as Vesta family (Hirayama 1918; Williams 1989; Nesvorný et al. 2015). This was reinforced by the discovery of two large impact craters in Vesta (Thomas et al. 1997; Marchi et al. 2012; Schenk et al. 2012; McSween et al. 2013, 2010). The link between most HED meteorites, V-type asteroids, and (4) Vesta is one of the best established in planetary science.

Another milestone for studies of V-type asteroids was the discovery of the basaltic nature of asteroid (1459) Magnya in early 2000 (Lazzaro et al. 2000). Based on dynamical investigation Michtchenko et al. (2002) suggested that this ~ 17 km (Delbo et al. 2006) asteroid located beyond 2.8 au from the Sun is most probably a part of other (than Vesta) planetesimal that existed in the outer parts of the

* E-mail: dagmara.oszkiewicz@amu.edu.pl

main belt. Hardersen, Gaffey & Abell (2004) further substantiated this claim by finding the discordant pyroxene chemistry of Magnya compared to that of Vesta. This showed that indeed there might be fragments of differentiated planetesimals other than Vesta in the Solar system supporting the hypothesis of multiple differentiated planetesimals.

More discoveries of such objects were made possible because of the start of a big survey era. Multiple studies focused on the search for V-type asteroids beyond 2.5 au in the middle and outer main belt (Roig & Gil-Hutton 2006; Moskovitz et al. 2008b; Roig et al. 2008; Duffard & Roig 2009; Solontoi et al. 2012; Oszkiewicz et al. 2014; Licandro et al. 2017; Medeiros et al. 2019; Mansour et al. 2020). About a dozen new V-types were found. Spectral studies showed that these objects similarly to Magnya are distinct from Vesta (Ieva et al. 2016, 2018; Leith et al. 2017). Furthermore, Roig et al. (2008) showed that large asteroids (>5 km) in the middle main belt region have a low probability of about ~1 per cent of having evolved from Vesta through a combination of the Yarkovsky effect and dynamical resonances. Ieva et al. (2018) suggest that the Eos asteroid family in the outer main belt could be the source of some of the V-types in this region. Dynamical evolution of V-type candidates also indicates that the parent bodies of the Eunomia and Merxia/Agnia families could also be a plausible source of V-types in the mid and outer main belt (Carruba et al. 2014). Similar origins are also suggested by Migliorini et al. (2021). On the other hand, Brasil et al. (2017) suggest the ‘jumping Jupiter’ planetary migration scenario as a possible transport mechanism from Vesta.

Theoretically, the number of V-type fragments originating from different planetesimals should be even greater in the inner Main belt (Bottke et al. 2006). However, most of the V-type asteroids in the inner main belt are part of the Vesta family or are considered fugitives, i.e. objects that evolved away from the family and are now beyond recognition as family members with traditional clustering methods. Early studies showed that some of the V-types in the inner main belt present a deeper 1.0 μm absorption bands than Vesta (Florczak et al. 2002). However, these findings were not confirmed by Ieva et al. (2016, 2018). Only one asteroid in the inner main belt, (2579) Spartacus, shows an unusually low band area ratio (BAR; ratio of the areas encompassed by the 1.0- and 2.0- μm absorption bands) compared to Vesta family members (Burbine et al. 2001; Moskovitz et al. 2010; Oszkiewicz et al. 2019). However, backward dynamical integration shows that the object could well originate from the Vesta family. Furthermore, BAR is often considered an unreliable parameter.

Basaltic material unrelated to Vesta is found in so-called anomalous meteorites (Yamaguchi, Setoyanagi & Ebihara 2006; McSween et al. 2010; Barrett et al. 2017; Zhang, Miao & He 2019) and micrometeorites (Gounelle et al. 2009). One of those falls was observed and its trajectory was traced back to the inner main belt (Bland et al. 2009; Spurný et al. 2012).

An unexpected place to find basaltic material was on the surface of carbonaceous asteroid (101955) Bennu. DellaGiustina et al. (2021) and Tatsumi et al. (2021) reported, based on data provided by OSIRIS-REx space mission, the identification of several bright boulders which showed the absorption bands characteristic of pyroxene composition, and their spectral features were matched by HED composition. At first glance, there is a dynamical similarity between the inner main belt basaltic asteroids and the source regions of Bennu (Tatsumi et al. 2021) which can explain how these boulders were implanted on Bennu. These findings provide new constraints on the collisional and dynamical evolution of the inner main belt.

Oszkiewicz et al. (2015, 2017) showed that some V-types in the inner main belt have spin orientation and thus Yarkovsky drift direction that is inconsistent with the origin in the Vesta family. However, strong evidence is still lacking, and the question of possible non-vestoids in the inner main belt is thus still under debate.

In this work, we identify V-type asteroids across the Solar system from *Gaia* Data Release 3 (DR3) spectral data. We analyse their spectral parameters in the context of multiple differentiated planetesimals. In Section 2, we describe the data used in the analysis and in Section 3 the methods used for spectral-type classification and spectral analysis. Results are presented in Section 4, discussion and conclusions are in Sections 5 and 6.

2 DATA

2.1 *Gaia* DR3 data

European Space Agency’s *Gaia* mission was launched in 2013 December. It operates at the Sun–Earth Lagrangian L2 point with the main goal of creating a 3D map of our Galaxy by surveying more than a billion stars (Prusti et al. 2016). *Gaia* measures the positions, proper motions, brightness, and spectra of objects crossing its fields of view, including asteroids (Mignard et al. 2007; Tanga & Mignard 2012; Tanga et al. 2022).

The current third data release (DR3) includes, for the first time, the mean reflectance spectra of 60 518 asteroids at visible wavelengths (0.374–1.05 μm), which is a 10-fold increase in the number of known asteroid spectra (Galluccio et al. 2022). This huge increase in the number of asteroid spectra is expected to result in a new taxonomic scheme (Delbo et al. 2012) and more detailed understanding of the distribution of various taxonomies across the Solar system and among asteroid families.

The *Gaia* spectral data are obtained by the blue and red photometers (BP/RP), which also cover the UV spectral region and are collectively referred to as XP instruments (Gaia Collaboration 2016; Prusti et al. 2016). Details of observations and data processing for asteroids are described in Galluccio et al. (2022). For each object, average spectra sampled at 16 wavelengths (in the range between 0.374 and 1.034 μm every 0.044 μm) together with 16 quality flags are provided. These spectra are the result of averaging typically more than 20 individual epoch spectra for each object (Galluccio et al. 2022). One epoch corresponds to a single transit of an asteroid in the *Gaia* focal plane.

2.2 Training data set

We classify asteroids into Bus-DeMeo classes (DeMeo et al. 2009) using three different supervised methods (see Section 3), which require a training data set. For that purpose, we used the collection of 3057 taxonomic labels from ground-based visible spectra from Mahlke, Carry & Mattei (2022). Those labels were then cross-matched by asteroid number or designation with objects observed by the *Gaia* mission leading to a sample containing 149 V-types and 2908 other-type asteroids (Fig. 1).

By using the *Gaia* data itself as a training set we teach the algorithms to recognize any possible systematic biases in the data that might be intrinsic to the *Gaia* mission. For example, the ground-based data are often obtained at opposition, thus at small phase angles. *Gaia* measurements are taken at phase angle >10 deg, this might result in moderate change of spectral slopes due to phase-reddening effect (Sanchez et al. 2012; Binzel et al. 2019).

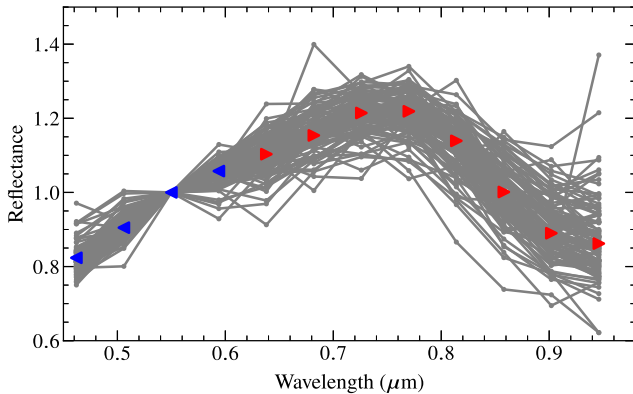


Figure 1. DR3 Spectra of 149 V-type asteroids used in the training process and their averaged spectra from the BP (blue) and RP (red) spectrometers. We marked average reflectances from BP and RP spectrometers in blue and red, respectively.

In the training parameter set, we omit reflectances at the wavelengths of 0.374, 0.418, 0.990, and 1.034 μm , as they are known to be affected by large random and systematic errors (Galluccio et al. 2022). We perform a linear regression using the remaining 12 points to obtain the spectral slope. This slope is removed from the spectra and treated as one of the parameters. Slope and slope-removed reflectances at the 12 wavelengths are then the final set of parameters for each spectra used in the training process. In Fig. 1, we show the V-type spectra used in training.

We also note that prior to using the *Gaia* DR3 data itself in the training process we experimented with several different training data sets from ground-based observations to simulated clones. The highest accuracy was reached when we used the DR3 spectra in the training process. We also inspected the predicted V-types visually to confirm the correctness of the results. We have assessed the influence of different parameters used in the classification task on the resulting accuracy as well. Using slope and reflectances versus only reflectances from raw (no slope removed) spectra resulted in a similar accuracy.

3 METHODS

3.1 Machine learning methods

We perform a binary classification into V-type versus other-types categories to increase the success rate. We use the three best-performing methods from Klimczak et al. (2021, 2022). We briefly summarize the methods below; for more details, see our recent works Klimczak et al. (2021, 2022).

(i) **Gradient Boosting (GB)** is a set of weak prediction methods. In particular, we use several decision trees. In each iteration, a new model is trained to minimize the residual left from the estimator from the previous stage (Hastie, Tibshirani & Friedman 2009).

(ii) **Support Vector Machines (SVM)** divide the feature space of different classes into separate regions with hyperplanes (Hastie et al. 2009). The algorithm maximises the width of the gap between the different classes.

(iii) **Multilayer Perceptrons (MLP)** we use a feedforward artificial neural network with two or three layers of perceptrons, each with 32 or 64 neurons. The weights of the neural connections are adjusted in a learning process with learning rates between 0.01 and 0.1 (Goodfellow, Bengio & Courville 2016).

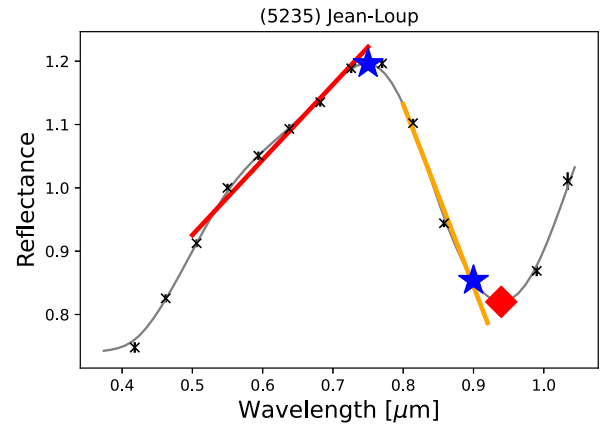


Figure 2. *Gaia* spectrum of (5235) Jean-Loup (black) and linear regression fits for wavelength ranges 0.5–0.75 μm (red, slope A) and 0.8–0.92 μm (orange, slope B). Grey line represents fitted cubic spline, reflectances at wavelengths used in computation of band depth are denoted with stars. Centre of the 0.9 μm absorption band is denoted with a diamond symbol. DR3 uncertainties are of the order of marker size.

We employ the implementation of methods from the PYTHON scikit-learn package (Pedregosa et al. 2011). To evaluate the algorithms, we use a balanced accuracy metric:

$$\text{BAcc} = \frac{1}{k} \sum_{i=1}^k \frac{\text{TP}_i}{\text{TP}_i + \text{FN}_i},$$

where k is the number of classes, TP_i ('true positives') is the number of correctly classified objects of class i , FP_i ('false positives') is the number of objects incorrectly classified in class i and FN_i ('false negatives') the number of incorrectly classified objects from class i . This metric gave the same general conclusions as unbalanced accuracy, F1 score, and Matthews correlation coefficient in our previous work (Klimczak et al. 2021) and is known to work well with imbalanced problems, as is the case in our study (Kelleher, Namee & D'Arcy 2015). To estimate the accuracy of the method, we use a 5-fold validation. That is, we divide the training set into 5 random parts. The algorithms are trained in 4 parts and evaluated in the 5th part. This process is repeated five times.

For the final prediction on new asteroids, the models are trained on the whole data set of 3057 objects, 149 of which are V-types.

3.2 Spectral parameters

To analyse the *Gaia* spectra of classified V-type asteroids in a consistent way with the literature (e.g. Ieva et al. 2016; Matlovič et al. 2020) we compute parameters that characterise the shape of the 0.9 μm absorption band on the original reflectances. In particular, for each spectrum we determine the reflectance gradient in the 0.5–0.75 μm range (slope A), the reflectance gradient in the 0.8–0.92 μm (slope B), apparent depth and centre of the 0.9 μm band (B1). Steeper A-slopes are an indication of space weathering (Fulvio et al. 2012, 2016) and a higher band depth relates to a larger grain size, the presence of fresh/unweathered pyroxene, or a different mineralogy (Cloutis et al. 2013). Gradients are computed as the slopes of the linear regression performed in the given wavelength ranges.

To estimate the band depth, we fit cubic splines to all *Gaia* points and then compute the reflectance at 0.75 and 0.9 μm (apparent depth) and their ratio. Minimum of the 0.9 μm band is found as the minimum of the fitted smoothing spline. In Fig. 2, we illustrate the parameters

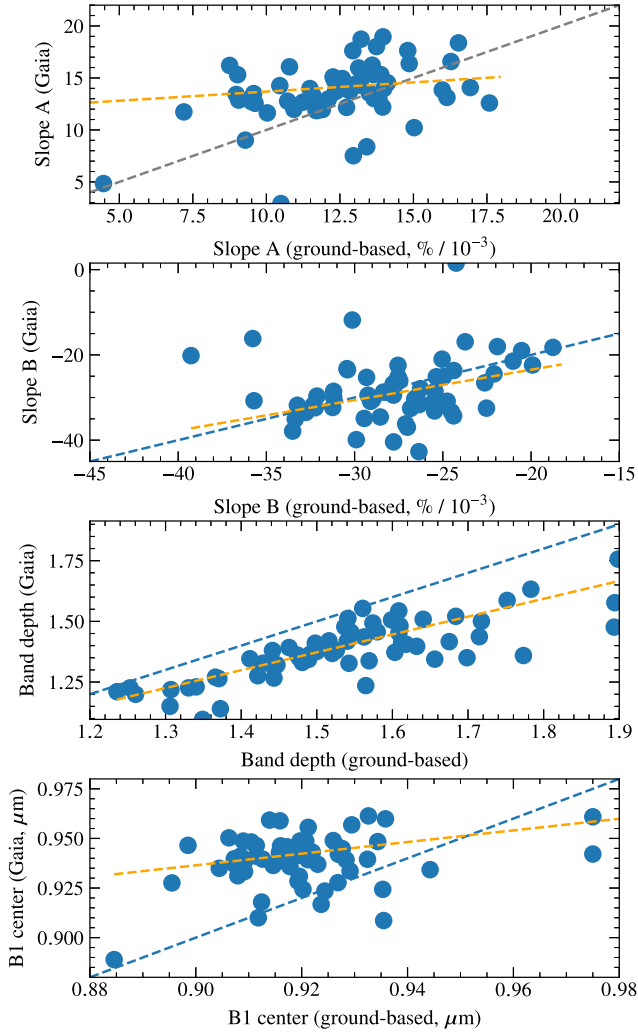


Figure 3. Comparison of spectral slopes, band depths, and centres for ground-based and *Gaia* observations of V-type asteroids. The dashed blue and orange lines represent the 1:1 relation, and a linear regression on the sample, respectively.

for the spectrum of a V-type asteroid, (5235) Jean-Loup. The derived parameters for this object are slope A = 11.9 per cent/ 10^3 \AA , slope B = -28.7 per cent/ 10^3 \AA , band depth = 1.41.

Galluccio et al. (2022) found that *Gaia* slightly underestimates the depth of the $0.9 \mu\text{m}$ absorption band and the spectral slope of V-types compared to the SMASSII survey (Bus & Binzel 2002). Furthermore, a systematic reddening of the UV part of the DR3 spectra as compared to the ground-based observations was found by Tinaut-Ruano et al. (in preparation). This reddening was contributed to the choice of solar analogue used to reduce the DR3 spectra (Tinaut-Ruano et al., in preparation). At the red part of the spectrum the choice of solar analogue was found not to affect the asteroid spectra. However differences wrt ground-based observations in this part of the spectrum are also known to exist. To verify this we compare spectral slopes, band depths, and band centres estimated from ground-based observations from Mahlke et al. (2022) with those obtained by the *Gaia* mission. In Fig. 3, we present the spectral parameters (slope A, slope B, $0.9 \mu\text{m}$ band depth and centre) for V-types present in both data sets. Distribution of slope A and slope B correlate with the ground-based data and there is no significant systematic bias. However, the DR3 slopes seems to be overestimated

for objects with small ground-based slope values and underestimated for objects with larger ground-based slope values. Band depth, on the other hand, is indeed systematically underestimated for all asteroids by about 0.15. Band centres seem to be overestimated for most objects. The linear relations between the DR3 and ground-based spectra are:

$$\text{slope}_A^{\text{DR3}} = 0.323 \times \text{slope}_A^{\text{grb}} + 9.975$$

$$\text{slope}_B^{\text{DR3}} = 0.713 \times \text{slope}_B^{\text{grb}} - 9.207$$

$$\text{apparent depth}^{\text{DR3}} = 0.679 \times \text{apparent depth}^{\text{grb}} + 0.349$$

$$\text{BI center}^{\text{DR3}} = 0.188 \times \text{BI center}^{\text{grb}} + 0.767,$$

where the upper indices denote the *Gaia* (DR3) and ground-based (grb) parameters. To determine the linear fits we have used the RANSACRegressor from the SKLEARN package with 3σ clipping. Generally, the spectra are internally consistent and thus can be internally compared.

3.3 Validation of V-type candidates

We follow a two-level validation. For the selection of V-type candidates, we require that the DR3 quality flags for all used wavelengths are validated. Additionally, all the predicted V-types from the full sample in the middle main belt, outer main belt, and the Phocaea and Hungaria regions are validated visually and added to the validated sample.

For the analysis of spectral parameters we require that the average signal-to-noise $\text{SNR} > 40$ and the DR3 spectral quality flags are validated for the wavelengths used in parameter estimation.

4 RESULTS

Based on the training data set and the 5-fold validation, we found a high success rate for the three methods. The resulting balanced accuracy was 92, 92, and 91 per cent for GB, SVM, and MLP, respectively. For comparison, spectrophotometric surveys typically reach accuracy of about 80 per cent (Klimczak et al. 2022). These relatively high classification scores are not surprising. The accuracy of classifying objects as V-types is typically very high due to the unique V-type spectra (see e.g. Moskovitz et al. 2008a; Oszkiewicz et al. 2014; Klimczak et al. 2021; Penttilä et al. 2021). Note also that neural networks and naive Bayes methods were already trained in preparation for *Gaia* data by Torppa et al. (2018) and Penttilä et al. (2021) also with very good results. Some misclassification occurs for Q/S-complex asteroids and objects with poor quality *Gaia* spectra. Some rare types with $0.9 \mu\text{m}$ band such as A, R, and O-type might also be misclassified as V-types. This is natural as many of the taxonomic types start to differ more in the near-infrared (NIR) part of the spectrum which is not observed by *Gaia*. These rare types, however, are scarce and should not pollute our sample significantly. Furthermore, R and A-types may also be linked to differentiated parent bodies (Moskovitz et al. 2008b; Sanchez et al. 2014; DeMeo et al. 2019).

Generally all methods predicted roughly a similar number of V-types, but GB predicted the fewest and SVN highest number of V-types. By visual inspection we noticed that a small portion of the V-types predicted by SVN (especially those that have poor quality spectra) may be misclassified. This might be due to the fact that SVN divides the parameter space by hyperplanes, which are difficult to find for categories split by highly non-linear boundaries. We also compared the predicted V-types with those predicted by Popescu et al. (2018) based on NIR spectrophotometry from the MOVIS

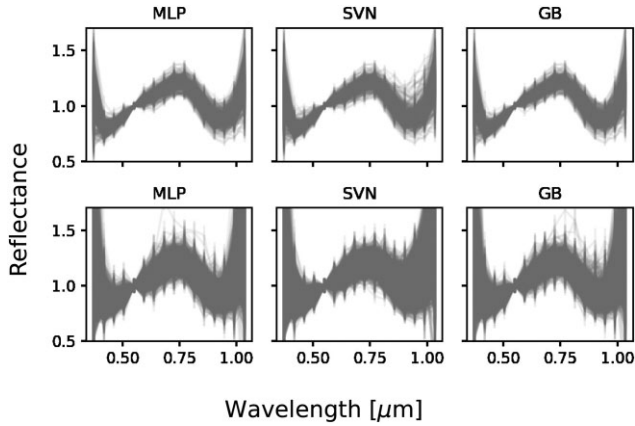


Figure 4. Spectra (normalized to unity at $0.55 \mu\text{m}$) of all the classified as V-types with MLP (left), SVM (middle), and GB (right), both in the validated (top) and full sample (bottom).

survey. We found 157 objects in common, out of which 151 were classified as V-types based Y , J , H , and K_s observations by Popescu et al. (2018) confirming the high prediction rate. Objects identified earlier by Popescu et al. (2018) based on the MOVIS survey data are marked in Table S1. As a side note, observe that the NIR MOVIS data are highly complementary in the wavelength ranges to the *Gaia* DR3 VIS spectroscopy.

In Fig. 4, we display spectra of all the classified objects. Top panel represents the validated spectra (all quality flags validated) and in the bottom panel we show all spectra classified as V-type irrespective of quality flags. Note that for some objects reflectance at $0.55 \mu\text{m}$ (normalization point) is flagged as invalid. Naturally, there is a larger spectral variability in the full sample.

We further split the two data sets into different populations in a consistent way with the literature (Ieva et al. 2016, 2018) based on orbital parameters, semimajor axis a , eccentricity e , and inclination i :

(i) Inner main belt ($2.1 \text{ au} < a \leq 2.5 \text{ au}$):

(a) Vestoids: members of the dynamical Vesta family as defined by the hierarchical clustering method by Nesvorný (2012)

(b) Fugitives: objects outside the dynamical Vesta family having $2.1 \text{ au} < a \leq 2.3 \text{ au}$, $5^\circ < i < 8^\circ$, and $0.035 < e < 0.162$

(c) Low- i : objects outside the dynamical Vesta family having $2.3 \text{ au} < a \leq 2.5 \text{ au}$ and $i < 6^\circ$

(d) Phocaea: with inclination above the ν_6 resonance, $2.5 \text{ au} > a > 2.25 \text{ au}$, $e > 0.1$ and $32^\circ > i > 18^\circ$

(e) Hungaria: $2.0 \text{ au} > a > 1.78 \text{ au}$, $32^\circ > i > 16^\circ$, $e < 0.18$

(f) Inner other: remaining objects in the inner main belt

(ii) Middle main belt ($2.5 \text{ au} < a \leq 2.82 \text{ au}$)

(iii) Other main belt ($2.82 \text{ au} < a < 3.2 \text{ au}$)

This division is illustrated for all validated V-types in Fig. 5. In Table 1, we report the number of classified V-types per population in the full and validated samples. Classifications made on spectra that is not fully validated should be treated as preliminary and confirmed visually. Interestingly, in the full sample we classified a number of new V-types in the mid and outer main belt (MOVs). Since MOVs are typically considered unrelated to Vesta, and are thus key in understanding the number of differentiated planetesimals, we further inspect the predicted V-type spectra visually. We confirm 11

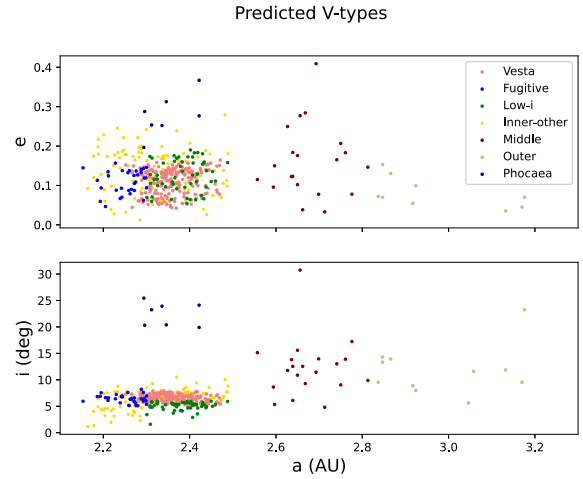


Figure 5. Distribution of orbital parameters of validated predicted V-types.

Table 1. The total number of new classified V-types in the validated and full sample (in brackets) per population.

Population/method	MLP	SVM	GB
Vesta	170 (907)	155 (853)	153 (762)
Fugitive	31 (187)	25 (157)	31 (156)
Low- i	47 (267)	49 (293)	46 (231)
Inner-other	105 (582)	104 (594)	98 (507)
Middle	16 (27)	19 (242)	16 (35)
Outer	10 (15)	10 (74)	7 (15)
Hungaria	0 (1)	0 (6)	0 (0)
Phocaea	5 (9)	4 (28)	3 (4)
Total:	384 (1995)	366 (2247)	354 (1710)

new V-types in the outer main belt and 20 in the mid main belt. Their spectra are plotted in Figs 6 and 7. We note that asteroid (7459) Gilbertofranco was previously observed by Medeiros et al. (2019) and is a confirmed eucritic V-type. That object was not present in our training sample and was correctly classified as V-type by all three algorithms. Intriguingly, in the full sample we find several V-types in the Phocaea and Hungaria regions that is primarily dominated by S and X-type objects with a minor percentage of other types (Carvano et al. 2001; Lucas et al. 2017, 2019). Phocaea dynamical group is considered a result of a collisional breakup of an ordinary chondrite-like body (Carvano et al. 2001; Carruba 2009). Therefore the predicted V-types are most likely interlopers. We investigate these predicted V-types in the Phocaea region visually and find six as V-types and one as A-type (Fig. 8). The A-type asteroid is (89776) 2002 AL90 and we remove this object from further analysis. In the Hungaria region none of the predicted V-types can be confirmed.

For the new V-types in the mid and outer-Main belt and in the Phocaea region we suggest further follow-up with ground-based telescopes since many of those are from the full sample with DR3 spectra that is not fully validated. In Figs 6–8 we marked the points with DR3 validation flag equal to 1 and 2 (poorer quality or compromised data) in orange and red, respectively. Some objects despite validated reflectance (e.g. 205560 except for a one point in UV) show a peculiar spectra. Many show the $0.9 \mu\text{m}$ absorption band, but do not strictly fit the ground-based templates for any taxonomic type. As discussed in Section 3.2 *Gaia* underestimates band depths and is burdened with systematic and random offsets as compared

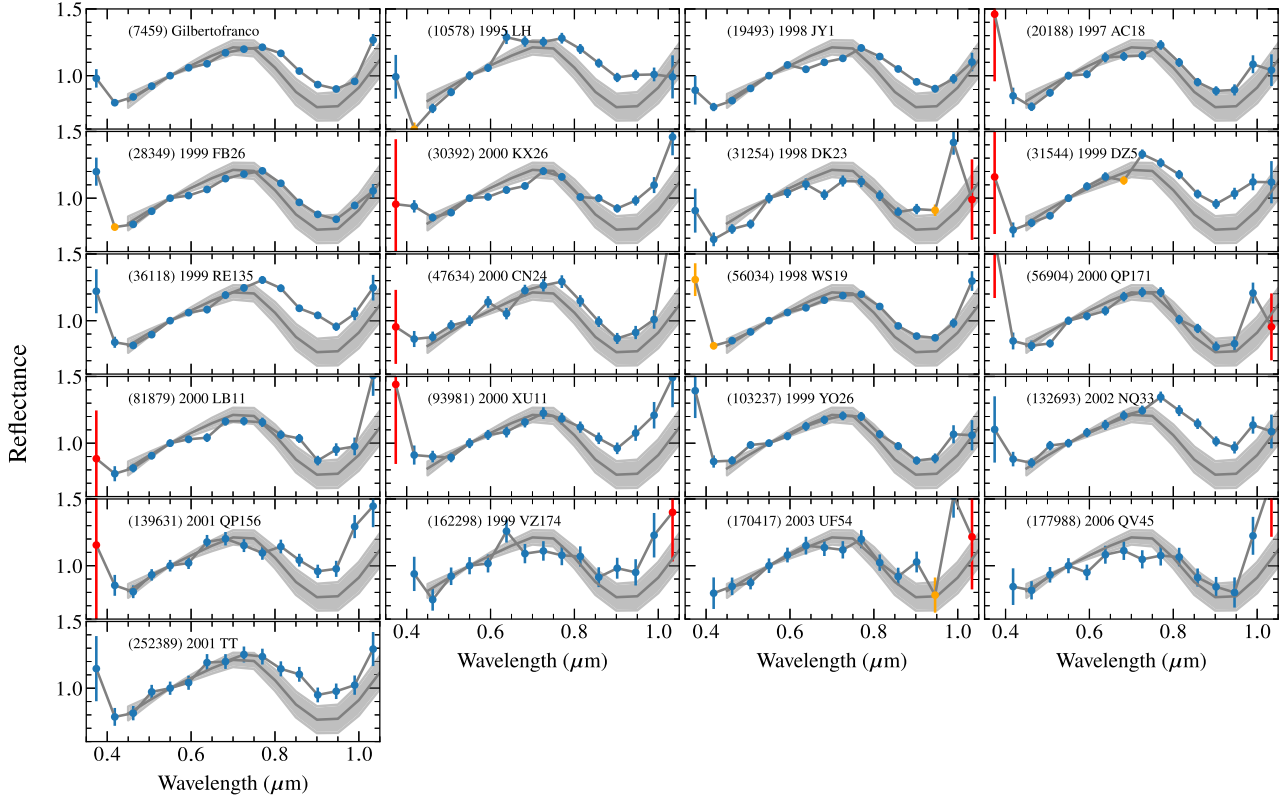


Figure 6. Examples of spectra of predicted V-types in the middle belt. DR3 validated reflectances are in blue and flagged points are in orange and red (DR3 reflectance_spectrum_flag equal to 1 and 2 correspondingly).

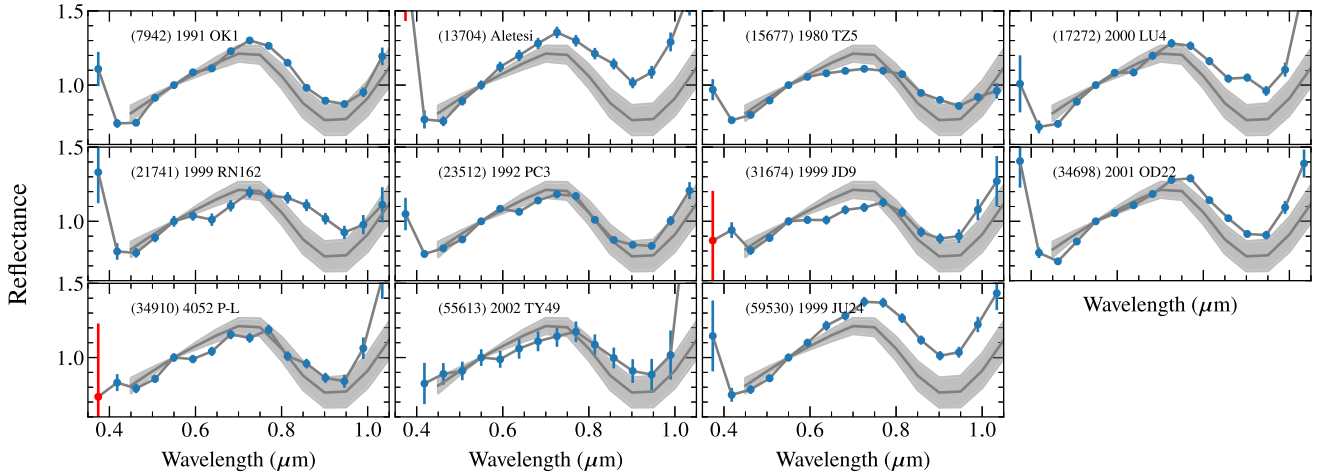


Figure 7. As in Fig. 6 but for the outer belt.

to the ground-based spectra, thus the DR3 data will not match the ground-based templates perfectly.

We further used the classified spectra to determine spectral parameters as described in Section 3. That is, we estimate slope A, slope B, apparent depth and centre of the 0.9 μm absorption band. In Figs 11–13, we plot the estimated spectral parameters for refined sample of objects with $\text{SNR} > 40$ and quality flags validated in the wavelength ranges of the investigated parameters. We include in this sample also the V-types known from the literature with DR3 spectra fulfilling the quality criteria. We remove objects for which band depth

is less than 1.2 from the analysis as those are often misclassified S-complex objects. In Table 2, we report the median values of slope A, slope B, 0.9 μm band depth and centre (B1 centre) for each population and learning algorithm. Overall the median values are consistent across the different algorithms. Median values of slope A, slope B, and band depth for the outer main belt population lie outside the one-standard-deviation (1σ) envelope of the Vesta family for all learning methods. Fugitives, low- i , and inner-other population have their average band depth outside or at the border of the 1σ envelope for the dynamical Vesta family members. Median B1

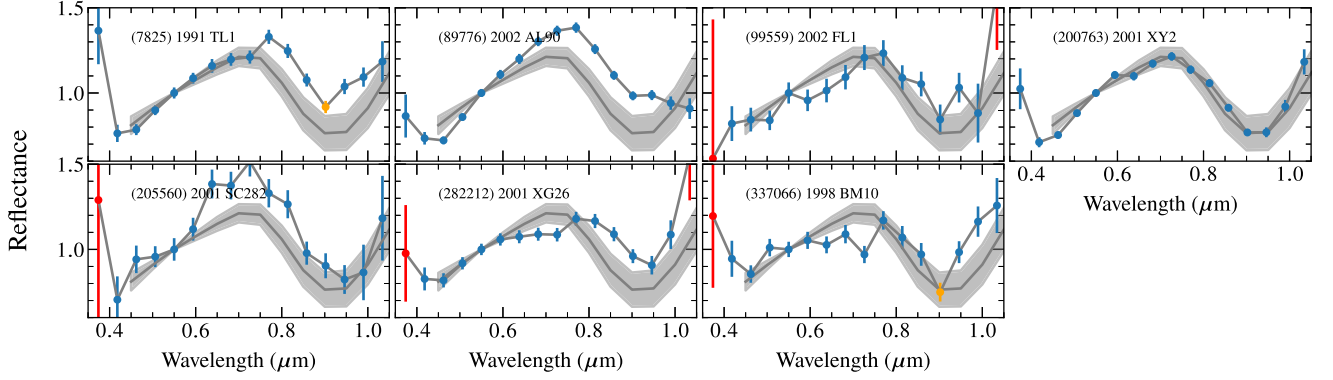


Figure 8. As in Fig. 6 but for the Phocaea region.

Table 2. Median values and standard deviations for slope A, slope B, 0.9 μm band depth and centre for different populations and learning algorithms in the validated sample.

Population	Slope A (per cent 10^{-3} \AA)	Slope B (per cent 10^{-3} \AA)	Band depth	B1 centre (μm)
MLP				
Vesta	12.56 ± 2.46	-26.11 ± 4.73	1.31 ± 0.09	0.93 ± 0.01
Fugitive	13.46 ± 2.31	-28.91 ± 5.14	1.40 ± 0.11	0.93 ± 0.02
Low- <i>i</i>	13.94 ± 1.85	-30.56 ± 5.35	1.43 ± 0.10	0.94 ± 0.01
Mid	12.36 ± 1.52	-25.73 ± 1.63	1.31 ± 0.06	0.94 ± 0.01
Outer	16.67 ± 3.70	-19.69 ± 6.38	1.41 ± 0.11	0.93 ± 0.01
Inner-other	13.76 ± 2.26	-28.32 ± 5.15	1.42 ± 0.12	0.94 ± 0.01
SVM				
Vesta	12.67 ± 2.45	-26.25 ± 4.65	1.32 ± 0.09	0.93 ± 0.01
Fugitive	13.52 ± 2.15	-29.87 ± 4.80	1.44 ± 0.10	0.93 ± 0.02
Low- <i>i</i>	14.21 ± 1.83	-30.56 ± 5.08	1.43 ± 0.10	0.94 ± 0.01
Mid	12.18 ± 2.20	-25.19 ± 2.21	1.29 ± 0.01	0.94 ± 0.01
Outer	16.67 ± 4.21	-20.34 ± 6.34	1.41 ± 0.10	0.92 ± 0.01
Inner-other	13.76 ± 2.21	-28.01 ± 5.29	1.42 ± 0.12	0.94 ± 0.01
GB				
Vesta	12.76 ± 2.33	-26.40 ± 4.74	1.33 ± 0.09	0.94 ± 0.01
Fugitive	13.49 ± 2.28	-29.20 ± 5.60	1.40 ± 0.12	0.93 ± 0.01
Low- <i>i</i>	13.96 ± 1.83	-30.56 ± 5.12	1.43 ± 0.10	0.94 ± 0.01
Mid	12.18 ± 2.20	-25.19 ± 2.21	1.29 ± 0.10	0.94 ± 0.01
Outer	16.92 ± 2.31	-22.49 ± 7.30	1.42 ± 0.10	0.93 ± 0.01
Inner-other	13.76 ± 2.19	-28.41 ± 5.20	1.42 ± 0.12	0.94 ± 0.01

centre, slope A and B for those populations are well within vestoidal values.

We find that the V-types from the outer main belt have band depths outside the 1σ envelope for the Vesta family members. This is consistent with the literature (Hardersen et al. 2004; Ieva et al. 2016; Leith et al. 2017; Ieva et al. 2018; Migliorini et al. 2018) and has been attributed to mineralogical differences before. Additional objects in this group with large band depths strengthen the finding that those objects are distinct from the fossil planetesimal (4) Vesta and Vesta family members. While most MOVs show larger apparent depth than typical vestoids, we also find objects [e.g. 15667 (5046 T-3) and 19493 (1998 JY1)] with a smaller band depth, more consistent with the spectra of (4) Vesta and vestoids. Additionally, one object from the middle main belt has spectral parameters well within typical vestoidal values. Two objects in the outer main belt (7942 and 34698), both at $a \sim 3.17$ au show similar spectral parameters. These objects are share similar semimajor axis and eccentricity, but vary in orbital inclination. Therefore a common origin would require presence of

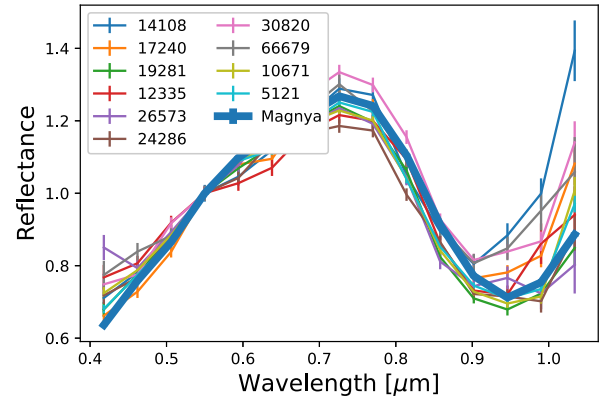


Figure 9. Spectra of selected V-types in the inner main belt with deep 0.9 μm absorption band more consistent with that of (1459) Magnya.

strong resonances near-by. This could be investigated with numerical studies.

In the inner main belt, there is large variability of spectral parameters for all populations. Fugitives, low-*i* and inner-other populations mostly overlap with the Vesta family objects in the spectral parameters space. Yet, a number of objects from those populations have band depths well outside the 2σ envelope of the Vesta family members. Furthermore, some of the objects have band depths even greater than that of (1459) Magnya. Few objects within the dynamical Vesta family also show spectral parameters well outside the 2σ envelope of the Vesta family. An exceptional example is asteroid 26573 with band depth more consistent with that of Magnya. We display the spectra of several such objects in Fig. 9.

Lithological differences between the vestoids and the low-*i* asteroids were reported previously by Mansour et al. (2020). Composition of one of those objects (19281) was investigated before with ground-based visible to near-infrared (VISNIR) wavelengths observations by Medeiros et al. (2019). Note also that this object was not in our training sample and was correctly identified by the machine-learning algorithms as a V-type object. The ground-based spectra shows indeed large 0.9 μm band depth. However, based on the 0.9 μm and the 2.0 μm band centres the authors concluded that this object is likely a former Vesta family member. One of the conclusions of Medeiros et al. (2019) was that compositional interpretations should rely on diagnostic plots that do not suffer from variability under slope removal. The authors recommended analysis of 0.9 μm and 2.0 μm band centres as the right diagnostic tool. For this reason we decided to compute also centres of the 0.9 μm band (Fig. 13). Most asteroids

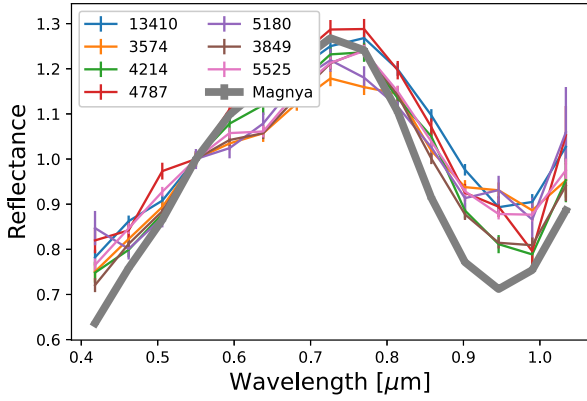


Figure 10. Spectra of selected V-types in the inner main belt with 0.9 μm absorption band centre at larger wavelengths.

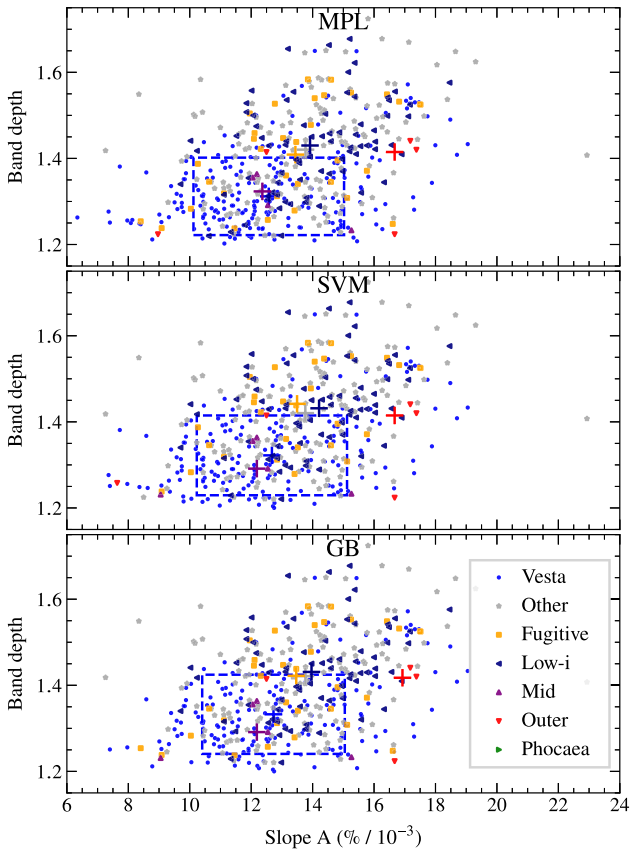


Figure 11. Slope A and apparent band depth for the V-type classified with MLP, SVM, GB methods and objects labelled in the literature. Different populations are marked with different colours and markers. Median values for the Slope A and band depth are denoted with crosses for each population. Blue frame represents 1σ envelope for the Vesta family members.

from the inner main belt have their 0.9 μm band centres well within typical vestoid values.

Objects with B1 centre larger than 1.0 μm are typically asteroids with what either appears to be erroneous DR3 spectra beyond 0.9 μm or incorrect taxonomic classification (i.e. 89 776 for which the minima is not reached by the spectrum and could be an olivine-dominated A-type asteroid). However, we also found asteroids with valid DR3 spectra having the B1 center at longer wavelengths than

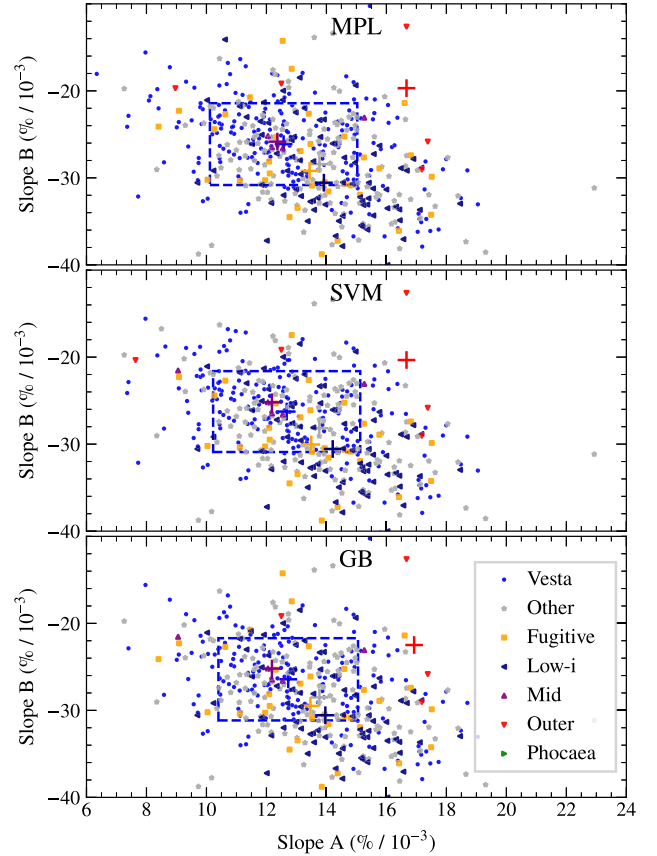


Figure 12. As in Fig. 11 but for Slope A and Slope B.

that of typical vestoids. DR3 spectra of some of those objects are plotted in Fig. 10. Two of those objects (5525, 3849) were previously observed (Xu et al. 1995; Bus & Binzel 2002; Oszkiewicz et al. 2020). For the first one, B1 centre is consistent with the ground-based observations, and for the latter one, it is overestimated.

Spectral parameters for all objects are listed in Table S2.

We further comment on the spectral parameters of asteroids with large band-depths as compared to the control sample from Ieva et al. (2016). The control sample in Ieva et al. (2016) was composed of vestoids observed at small phase angles ($1^\circ < \alpha < 12^\circ$). The sample bounded a confined region in spectral parameters phase space. Slope A was found to vary from 7.26 and 18.51 per cent 10^{-3} \AA , slope B from -35.98 to -18.41 per cent 10^{-3} \AA and band depth from 1.15 to 1.72. Since band depth is underestimated in the *Gaia* spectra (see Section 2) the upper limit for band depth for the *Gaia* spectra should be about 0.2 less than that from Ieva et al. (2016). This leaves a number of V-types from the inner main belt outside the region of spectral parameters bounded by the control sample from Ieva et al. (2016).

We conclude that indeed the inner main belt could be a mix of objects from various planetesimals, not just (4) Vesta. Number of identified asteroids with large 0.9 μm band depths or band centres offset from typical vestoids is however low. The differentiated planetesimals thus could have formed in a wider orbital range [e.g. 1.3 and 7.5 au from the Sun as indicated by (Lichtenberg et al. 2021)] as opposed to a narrow terrestrial planet region proposed by Bottke et al. (2006) which would lead to increased number of those objects in the inner main belt. It is also plausible that these objects remain spectrally indistinguishable from Vesta and Vesta family members.

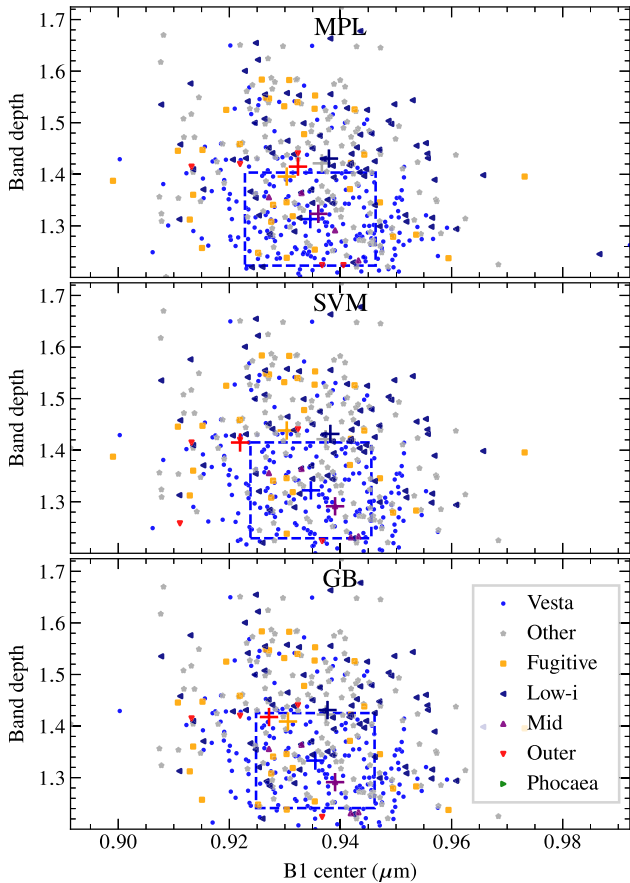


Figure 13. As in Fig. 11 but for band depth and band centre.

These objects should be followed-up by ground-based VISNIR spectroscopy at small phase angles for full mineralogical characterization.

5 DISCUSSION

The largest source of uncertainty in this work is the phase reddening effect (changes in spectral slope, colour indices, variations in albedo, and absorption bands depth with changing phase angle). Although known for decades, the effect has been studied in detail on a very limited number (less than several dozens) of objects (Millis, Bowell & Thompson 1976; Miner & Young 1976; Clark et al. 2002; Reddy et al. 2012; Sanchez et al. 2012) and for only a few taxonomic types. Moreover, the effect has been suggested to differ from asteroid to asteroid by Binzel et al. (2019), Carvano & Davalos (2015). A limited laboratory work also demonstrated the effect on various analogues of planetary material (Gradie, Veverka & Buratti 1980; Gradie & Veverka 1986).

Since average phase angles are not reported with the *Gaia* spectra, correcting for this effect is not possible. Moreover, a single *Gaia* spectra is obtained from averaging spectra from multiple transits, thus from multiple phase angles, therefore correcting for phase reddening becomes non-trivial.

Median phase angle for an average *Gaia* spectra is about 20 deg (whereas the ground-based observations are typically taken at opposition, close to 0 deg) thus there is a concern of phase reddening affecting the obtained asteroid spectra (Cellino et al. 2020; Galluccio et al. 2022). At these phase angles phase reddening is expected to

Table 3. Future observing opportunities for selected inner-main Belt V-types. Columns are: asteroid number, designation, date of the next opposition, declination and predicted *V*-magnitude at the nearest opposition.

Number	Designation	Next opp.	Dec. (deg)	<i>V</i> (mag)
13410	1999 UX5 Arhale	2022/12/19	+22	17.4
3574	1982 TQ Rudaux	2023/08/03	−09	16.0
4214	1987 UX4 Veralynn	2023/05/02	−18	16.2
4787	1986 RC7 Shul’zhenko	2023/07/17	−30	16.1
5180	1989 GF Ohno	2023/07/18	−27	16.8
3849	1984 FC Incidentia	2023/04/12	−08	16.0
5525	1991 TS4	2023/03/16	−01	16.4
14108	1998 OA13	2022/09/09	+01	16.3
172240	2002 RO19	2023/05/23	−15	20.2
19281	1996 AP3	2022/08/04	−08	15.3
12335	1992 WJ3 Tatsukushi	2023/09/04	−05	16.9
26573	2000 EG87	2022/09/20	+03	15.8
24286	1999 XU18	2023/08/26	−12	16.0
30820	1990 RU2	2022/08/19	−19	16.7
66679	1999 TD29	2022/10/27	+10	17.4
10671	1977 RR6 Mazurova	2023/12/23	+32	16.8
5121	1989 AX1 Numazawa	2023/04/10	−11	16.5
19281	1996 AP3	2022/08/04	−08	15.3

increase spectral slopes and band depths of V-type asteroids (Reddy et al. 2012).

Based on satellite observations of a single object (4) Vesta, Reddy et al. (2012) found around 20 per cent increase in overall spectral slope for every 10 deg increase of phase angle and 2.35 per cent increase of the band depth of 0.9 μm absorption band. Since band depth are not influenced significantly, our conclusions for inner main belt V-types with large absorption bands would still hold. Furthermore, we found that band depths are systematically underestimated in the *Gaia* spectra, thus they may be even larger than estimated.

Ieva et al. (2016, 2018) used the relation from Reddy et al. (2012) to correct the spectral parameters of V-types for phase reddening, but also noted that the correction is more qualitative than quantitative. Since band depths are not significantly affected, the same conclusions would have been reached without the correction.

Other effects such as space weathering and regardening have less impact on our conclusions. Space weathering is expected to lower band-depths (Vernazza et al. 2006; Fulvio et al. 2012) and regardening is acting on near-Earth asteroids (Binzel et al. 2010).

Another source of concern are the unknown systematic and random errors of the *Gaia* spectra. The *Gaia* mission was designed for stellar tracking. Spectra for moving objects such as asteroids is extracted from windows that are moving at stellar rates. Since the XP spectra is taken at the end of the transit the difference between the actual asteroid position and the position of the window is the largest (Galluccio et al. 2022). Complicated wavelength calibration can cause further uncertainties (Galluccio et al. 2022). As noted in Section 2 DR3 spectra tends to underestimate band depth for V-type asteroids. Galluccio et al. (2022) estimated the average difference between SMASS II and DR3 *z*−*i* colour across all taxonomic types to be about −0.08 and derived formulas for correcting the *z*−*i* colour and overall spectral slope to the SMASS II data set.

These formulas are however more applicable to population studies and not to individual objects, due to large variability of the correction. Furthermore, the V-type asteroids seem to be affected more by this systematic effect than other taxonomic types (Galluccio et al. 2022).

Table 4. As in Table 3 but for objects in the mid main belt.

Number	Designation	Next opp.	Dec. (deg)	V (mag)
10578	1995 LH	2022/11/30	+28	18.0
28349	1999 FB26	2023/05/07	-29	17.9
81879	2000 LB11	2023/06/02	-08	18.3
36118	1999 RE13	2022/11/06	+09	17.4
170417	2003 UF54	2023/01/23	+03	19.6
139631	2001 QP15	2023/05/27	-01	20.1
30392	2000 KX26	2023/10/02	+21	18.1
252389	2001 TT	2022/10/05	-35	19.6
93981	2000 XU11	2023/01/06	+37	17.9
19493	1998 JY1	2023/03/14	-04	17.7
47634	2000 CN24	2023/06/25	-06	18.4
56904	2000 QP17	2022/11/11	+01	18.9
7459	1984 HR1 Gilbertofranco	2023/10/29	+13	16.8
20188	1997 AC18	2023/06/25	-21	17.0
132693	2002 NQ33	2023/04/28	-29	18.8
177988	2006 QV45	2023/09/01	-05	19.3
103237	1999 YO26	2023/10/25	+20	17.2

Table 5. As in Table 3 but for objects in the outer main belt.

Number	Designation	Next opp.	Dec. (deg)	V (mag)
7942	1991 OK1	2023/02/13	+ 09	16.4
15677	1980 TZ5	2023/09/10	-18	15.6
23512	1992 PC3	2023/05/07	-29	17.1
34910	4052 P-L	2023/04/08	-10	18.7
55613	2002 TY49	2022/11/21	+ 20	18.3
59530	1999 JU24	2023/09/28	-06	17.5
23512	1992 PC3	2023/05/07	-29	17.1
13704	1998 PA1 Aletesi	2023/05/01	-17	18.5
21741	1999 RN16	2023/09/10	-23	17.2
17272	2000 LU4	2023/03/27	+ 08	17.7

Table 6. As in Table 3 but for objects in the Phocaea region.

Number	Designation	Next opp.	Dec. (deg)	V (mag)
7825	1991 TL1	2023/04/21	-04	17.2
89776	2002 AL90	2022/09/07	-18	17.4
99559	2002 FL1	2023/03/25	+ 02	16.8
205560	2001 SC28	2023/01/03	-11	17.7
282212	2001 XG26	2022/11/04	-33	17.9
337066	1998 BM10	2022/09/19	-29	21.2

The ground-based spectral observations over the visible and near-infrared wavelengths will allow a detailed characterization of the most interesting targets reported in this work, namely asteroids from Figs 9 and 10 in the inner main belt as well as all potential V-types in the mid and outer main belt reported in Table S1. For observers convenience we list the dates of nearest oppositions, predicted V-magnitude, and declination at opposition for the interesting objects in Tables 3–6.

6 CONCLUSIONS

We classified 60 518 asteroids from the *Gaia* DR3 catalogue into V-types and non-V-types. We found about 2000 new V-types and validated around 350 of them. We found 31 new V-types in the mid and outer main belt and 6 in the Phocaea region. This adds to the inventory of objects that are not easily linked to the fossil planetesimal (4) Vesta. We suggest further follow-up of those objects

by ground-based observations to fully confirm their basaltic nature. Large number of V-types is found in the inner main belt.

For the first time, we found a number of objects in the inner main belt with large band depths, some even larger than that of (1459) Magnya. We also found objects with 0.9 μm band centres offset from typical vestoidal values. However, band centers are randomly overestimated in the DR3 data thus are not reliable. Future asteroid spectroscopy to be provided in the *Gaia* DR4 catalogue may contain improved processing with spectra having less biases thus might also provide a better insight into the spectroscopic parameters of V-types.

We show that there are V-type asteroids in the inner main belt that may be distinct from Vesta. Further ground-based observations in the near-infrared are needed for full mineralogical analysis of those objects. Determination of spins and shapes accompanied with backward dynamical analysis may further provide evidence for existence of differentiated planetesimals in the inner main belt other than Vesta.

ACKNOWLEDGEMENTS

This work has been supported by grant no. 2017/26/D/ST9/00240 from the National Science Centre, Poland. HK was supported by grant no. 2017/25/B/ST9/00740 from the National Science Centre, Poland, and AP was supported by grant no. 325805 from the Academy of Finland. The work of MP was made in the framework of the project PN19-030102-INCDPM, contract number 21N/2019, MCID, Romania. This work has used data from the European Space Agency (ESA) mission *Gaia*¹. This work presents results from the European Space Agency (ESA) space mission, *Gaia*. *Gaia* data are being processed by the *Gaia* Data Processing and Analysis Consortium (DPAC). Funding for the DPAC is provided by national institutions, in particular the institutions participating in the *Gaia* MultiLateral Agreement (MLA). The *Gaia* mission website is <https://www.cosmos.esa.int/gaia>. The *Gaia* archive website is <https://archives.esac.esa.int/gaia>.

DATA AVAILABILITY

This research used publicly available data from the DR3 catalogue of the European Space Agency mission *Gaia*. Tables S1 and S2 will be provided in a numerical form though CDS after publication.

REFERENCES

- Barrett T. et al., 2017, *Meteorit. Planet. Sci.*, 52, 656
 Binzel R. P., Xu S., 1993, *Science*, 260, 186
 Binzel R. et al., 2019, *Icarus*, 324, 41
 Binzel R. P. et al., 2010, *Nature*, 463, 331
 Bland P. A. et al., 2009, *Science*, 325, 1525
 Botke W. F., Nesvorný D., Grimm R. E., Morbidelli A., O'Brien D. P., 2006, *Nature*, 439, 821
 Brasil P., Roig F., Nesvorný D., Carruba V., 2017, *MNRAS*, 468, 1236
 Burbine T. H., Buchanan P. C., Binzel R. P., Bus S. J., Hiroi T., Hinrichs J., Meibom A., McCoy T. J., 2001, *Meteorit. Planet. Sci.*, 36, 761
 Burbine T. H., McCoy T. J., Meibom A., Gladman B., Keil K., 2002, *Asteroids III*, The University of Arizona Press, Tucson, AZ
 Bus S. J., Binzel R. P., 2002, *Icarus*, 158, 146
 Carruba V., 2009, *MNRAS*, 398, 1512
 Carruba V., Huaman M., Domingos R., Santos C. D., Souami D., 2014, *MNRAS*, 439, 3168

¹<https://www.cosmos.esa.int/gaia>

- Carvano J. M., Davalos J., 2015, *A&A*, 580, A98
- Carvano J. M., Lazzaro D., Mothé-Diniz T., Angeli C. A., Florczak M., 2001, *Icarus*, 149, 173
- Cellino A., Bendjoya P., Delbo M., Galluccio L., Gayon-Markt J., Tanga P., Tedesco E., 2020, *A&A*, 642, A80
- Clark B. E. et al., 2002, *Icarus*, 155, 189
- Cloutis E. et al., 2013, *Icarus*, 223, 850
- Delbo M. et al., 2006, *Icarus*, 181, 618
- Delbo M. et al., 2012, *Planet. Space Sci.*, 73, 86
- DellaGiustina D. N. et al., 2021, *Nat. Astron.*, 5, 31
- DeMeo F. E., Binzel R. P., Slivan S. M., Bus S. J., 2009, *Icarus*, 202, 160
- DeMeo F. E., Polishook D., Carry B., Burt B. J., Hsieh H. H., Binzel R. P., Moskovitz N. A., Burbine T. H., 2019, *Icarus*, 322, 13
- Duffard R., Roig F., 2009, *Planet. Space Sci.*, 57, 229
- Florczak M., Lazzaro D., Duffard R., 2002, *Icarus*, 159, 178
- Fulvio D., Brunetto R., Vernazza P., Strazzulla G., 2012, *A&A*, 537, L11
- Fulvio D., Perna D., Ieva S., Brunetto R., Kanuchova Z., Blanco C., Strazzulla G., Dotto E., 2016, *MNRAS*, 455, 584
- Gaia Collaboration, 2016, *A&A*, 595, A2
- Galluccio L. et al., 2022, *A&A* (forthcoming), preprint ([arXiv:2206.12174](https://arxiv.org/abs/2206.12174))
- Goodfellow I. J., Bengio Y., Courville A., 2016, *Deep Learning*. MIT Press, Cambridge, MA, USA
- Gounelle M., Chaussidon M., Morbidelli A., Barrat J.-A., Engrand C., Zolensky M. E., Mckeegan K. D., 2009, *Proc. Natl. Acad. Sci.*, 106, 6904
- Gradie J., Veverka J., 1986, *Icarus*, 66, 455
- Gradie J., Veverka J., Buratti B., 1980, *Lunar and Planetary Science Conference Proceedings*, 11, 799–815
- Greenwood R. C. et al., 2015, *Geochim. Cosmochim. Acta*, 169, 115
- Hardersen P. S., Gaffey M. J., Abell P. A., 2004, *Icarus*, 167, 170
- Hastie T., Tibshirani R., Friedman J., 2009, *The Elements of Statistical Learning: Data Mining, Inference and Prediction*, 2 edn. Springer, New York, available at <http://www-stat.stanford.edu/tibs/ElemStatLearn/>
- Hirayama K., 1918, *Groups of asteroids probably of common origin*, *The Astronomical Journal*, 31, 185–188
- Hunt A. C., Theis K. J., Rehkämper M., Benedix G. K., Andreassen R., Schönbachler M., 2022, *Nat. Astron.*, 6, 812–818
- Ieva S., Dotto E., Lazzaro D., Perna D., Fulvio D., Fulchignoni M., 2016, *MNRAS*, 455, 2871
- Ieva S., Dotto E., Lazzaro D., Fulvio D., Perna D., Mazzotta Epifani E., Medeiros H., Fulchignoni M., 2018, *MNRAS*, 479, 2607
- Kelleher J. D., Namee B. M., D’Arcy A., 2015, *Fundamentals of Machine Learning for Predictive Data Analytics: Algorithms, Worked Examples, and Case Studies*. MIT Press, Cambridge, MA, USA
- Klimczak H., Kotłowski W., Oszkiewicz D. A., DeMeo F., Kryszczyńska A., Wilawer E., 2021, *Front. Astron. Space Sci.*, 8, 216
- Klimczak H., Oszkiewicz D., Benoit C., Penttilä A., Kotłowski W., Kryszczyńska A., Emil W., 2022, *A&A*, 667, A10
- Lazzaro D. et al., 2000, *Science*, 288, 2033
- Leith T. B., Moskovitz N. A., Mayne R. G., DeMeo F. E., Takir D., Burt B. J., Binzel R. P., Pefkou D., 2017, *Icarus*, 295, 61
- Licandro J., Popescu M., Morate D., de León J., 2017, *A&A*, 600, A126
- Lichtenberg T., Drązkowska J., Schönbachler M., Golabek G. J., Hands T. O., 2021, *Science*, 371, 365
- Lucas M. P. et al., 2019, *Icarus*, 322, 227
- Lucas M. P., Emery J. P., Pinilla-Alonso N., Lindsay S. S., Lorenzi V., 2017, *Icarus*, 291, 268
- Mahlke M., Carry B., Mattei P.-A., 2022, *A&A*, 665, A26
- Mansour J.-A., Popescu M., de León J., Licandro J., 2020, *MNRAS*, 491, 5966
- Marchi S. et al., 2012, *Science*, 336, 690
- Matlovič P., de León J., Medeiros H., Popescu M., Rizos J. L., Mansour J.-A., 2020, *A&A*, 643, A107
- McCord T. B., Adams J. B., Johnson T. V., 1970, *Sci*, 168, 1445
- McSween H. Y. Jr. et al., 2013, *Meteorit. Planet. Sci.*, 48, 2090
- McSween H. Y., Mittlefehldt D. W., Beck A. W., Mayne R. G., McCoy T. J., 2010, *The Dawn Mission to Minor Planets 4 Vesta and 1 Ceres*, Springer, New York, NY, p. 141
- Medeiros H. et al., 2019, *MNRAS*, 488, 3866
- Michtchenko T., Lazzaro D., Ferraz-Mello S., Roig F., 2002, *Icarus*, 158, 343
- Migliorini A., De Sanctis M., Lazzaro D., Ammannito E., 2018, *MNRAS*, 475, 353
- Migliorini A., De Sanctis M., Michtchenko T., Lazzaro D., Barbieri M., Mesa D., Lazzarin M., La Forgia F., 2021, *MNRAS*, 504, 2019
- Mignard F. et al., 2007, *Earth Moon Planets*, 101, 97
- Millis R., Bowell E., Thompson D., 1976, *Icarus*, 28, 53
- Miner E., Young J., 1976, *Icarus*, 28, 43
- Moskovitz N. A., Jedicke R., Gaidos E., Willman M., Nesvorný D., Fevig R., Ivezic Z., 2008a, *Icarus*, 198, 77
- Moskovitz N. A., Lawrence S., Jedicke R., Willman M., Haghighipour N., Bus S. J., Gaidos E., 2008b, *ApJ*, 682, L57
- Moskovitz N. A., Willman M., Burbine T. H., Binzel R. P., Bus S. J., 2010, *Icarus*, 208, 773
- Nesvorný D., 2020, *Nesvorný HCM Asteroid Families V1.0*. urn:nasa:pds:ast.nesvorny.families::1.0. NASA Planetary Data System. p. EAR–A
- Nesvorný D., Brož M., Carruba V., 2015, *Asteroids IV*, Vol. 29, The University of Arizona Press, Tucson, AZ, USA, p. 7
- Oszkiewicz D., Kwiatkowski T., Tomov T., Birlan M., Geier S., Penttilä A., Polińska M., 2014, *A&A*, 572, A29
- Oszkiewicz D., Kankiewicz P., Włodarczyk I., Kryszczyńska A., 2015, *A&A*, 584, A18
- Oszkiewicz D. et al., 2019, *A&A*, 623, A170
- Oszkiewicz D. et al., 2020, *A&A*, 643, A117
- Oszkiewicz D. A., Skiff B. A., Moskovitz N., Kankiewicz P., Marciniak A., Licandro J., Galiazzo M. A., Zeilinger W. W., 2017, *A&A*, 599, A107
- Pedregosa F. et al., 2011, *J. Mach. Learn. Res.*, 12, 2825
- Penttilä A., Hietala H., Muinonen K., 2021, *A&A*, 649, A46
- Popescu M., Licandro J., Carvano J., Stoicescu R., de León J., Morate D., Boacă I., Cristescu C., 2018, *A&A*, 617, A12
- Prusti T. et al., 2016, *A&A*, 595, A1
- Reddy V. et al., 2012, *Icarus*, 217, 153
- Roig F., Gil-Hutton R., 2006, *Icarus*, 183, 411
- Roig F., Nesvorný D., Gil-Hutton R., Lazzaro D., 2008, *Icarus*, 194, 125
- Sanchez J. A., Reddy V., Nathues A., Cloutis E. A., Mann P., Hiesinger H., 2012, *Icarus*, 220, 36
- Sanchez J. A. et al., 2014, *Icarus*, 228, 288
- Schenk P. et al., 2012, *Science*, 336, 694
- Scott E. R., Greenwood R. C., Franchi I. A., Sanders I. S., 2009, *Geochim. Cosmochim. Acta*, 73, 5835
- Scott E. R., Keil K., Goldstein J. I., Asphaug E., Bottke W. F., Moskovitz N. A., 2015, *Asteroids IV*. University of Arizona Press, Tucson, AZ, USA, p. 573
- Solontoi M. R., Hambergren M., Gyuk G., Puckett A., 2012, *Icarus*, 220, 577
- Spurný P. et al., 2012, *Meteorit. Planet. Sci.*, 47, 163
- Tanga P. et al., 2022, *A&A* Forthcoming, preprint ([arXiv:2206.05561](https://arxiv.org/abs/2206.05561))
- Tanga P., Mignard F., 2012, *Planet. Space Sci.*, 73, 5
- Tatsumi E. et al., 2021, *MNRAS*, 508, 2053
- Thomas P. C., Binzel R. P., Gaffey M. J., Storrs A. D., Wells E. N., Zellner B. H., 1997, *Science*, 277, 1492
- Torppa J. et al., 2018, *Adv. Space Res.*, 62, 464
- Vernazza P., Brunetto R., Strazzulla G., Fulchignoni M., Rochette P., Meyer-Vernet N., Zouganelis I., 2006, *A&A*, 451, L43
- Williams J., 1989, *Asteroids II*. University of Arizona Press, Tucson, AZ, USA, p. 1034
- Xu S., Binzel R. P., Burbine T. H., Bus S. J., 1995, *Icarus*, 115, 1
- Yamaguchi A., Setoyanagi T., Ebihara M., 2006, *Meteorit. Planet. Sci.*, 41, 863
- Zhang C., Miao B., He H., 2019, *Planet. Space Sci.*, 168, 83

SUPPORTING INFORMATION

Supplementary data are available at [MNRAS](#) online.

Table S1. Predicted V-types with the MLP, SVM, and GB methods and their orbital parameters (semimajor axis a , eccentricity e , and inclination i), prediction methods, validation flag (all DR3 points validated) and SNR.

Table S2. Orbital and spectral parameters of analyzed V-types.

Please note: Oxford University Press is not responsible for the content or functionality of any supporting materials supplied by the authors. Any queries (other than missing material) should be directed to the corresponding author for the article.

This paper has been typeset from a $\text{\TeX}/\text{\LaTeX}$ file prepared by the author.